



Cite this: *Dalton Trans.*, 2021, **50**, 3641

Site-selective protonation of the one-electron reduced cofactor in [FeFe]-hydrogenase†

Konstantin Laun,^{a,b} Iuliia Baranova,^{a,c} Jifu Duan,^d Leonie Kertess,^d Florian Wittkamp,^e Ulf-Peter Apfel,^d Thomas Happe,^d Moritz Senger^d *^{a,g} and Sven T. Stripp^d *^a

Hydrogenases are bidirectional redox enzymes that catalyze hydrogen turnover in archaea, bacteria, and algae. While all types of hydrogenase show H₂ oxidation activity, [FeFe]-hydrogenases are excellent H₂ evolution catalysts as well. Their active site cofactor comprises a [4Fe–4S] cluster covalently linked to a diiron site equipped with carbon monoxide and cyanide ligands. The active site niche is connected with the solvent by two distinct proton transfer pathways. To analyze the catalytic mechanism of [FeFe]-hydrogenase, we employ *operando* infrared spectroscopy and infrared spectro-electrochemistry. Titrating the pH under H₂ oxidation or H₂ evolution conditions reveals the influence of site-selective protonation on the equilibrium of reduced cofactor states. Governed by pK_a differences across the active site niche and proton transfer pathways, we find that individual electrons are stabilized either at the [4Fe–4S] cluster (alkaline pH values) or at the diiron site (acidic pH values). This observation is discussed in the context of the complex interdependence of hydrogen turnover and bulk pH.

Received 12th January 2021,
Accepted 21st February 2021

DOI: 10.1039/d1dt00110h
rsc.li/dalton

[FeFe]-Hydrogenases are gas-processing metalloenzymes that have been found in bacteria and green algae.^{1–4} They serve various roles in the hydrogen metabolism of prokaryotes, including oxidation of H₂ as an energy carrier and proton reduction (H₂ evolution) to maintain the cellular redox equilibrium.⁵ In the chloroplast of green algae, they are part of the photosynthetic electron transport chain, coupling H₂O oxidation and H₂ evolution at the reducing end of photosystem I.⁶ The first crystal structures of [FeFe]-hydrogenase helped identifying accessory and catalytic iron-sulfur clusters as well as gas channels and potential proton transfer (PT) pathways.^{7–13} Additionally, various biophysical techniques were employed to characterize the electronic structure of the active site cofactor, the so-called ‘H-cluster’ (Fig. 1).¹ This iron-sulfur compound is

formed by a [4Fe–4S] cluster connected to a bimetallic iron site *via* a bridging cysteine residue. The diiron site has been shown to bind carbon monoxide (CO) and cyanide ligands (CN[–]) that are a unique feature of hydrogenase.^{14–16} The aminothiolate ligand (ADT) that bridges the metal ions of the diiron site was suggested to act as an inner-sphere hydrogen-bonding donor to a number of apical ligands at the distal iron ion (Fe_d).¹⁷

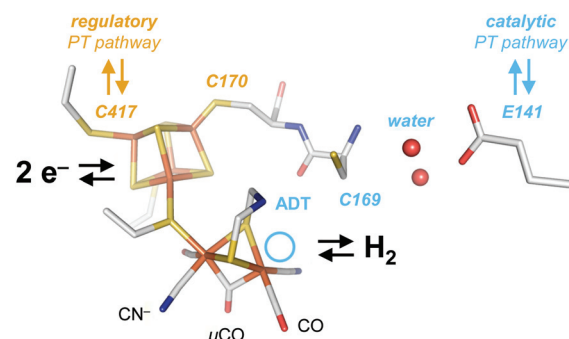


Fig. 1 Cofactor and active site niche. The H-cluster comprises a [4Fe–4S] cluster linked to the catalytic diiron site. In the crystallized Hox state, the H-cluster carries two terminal CO and CN[–] ligands and a single μCO ligand (pdb ID 4XDC). The ADT ligand serves as a proton relay between the distal iron ion (Fe_d) and the catalytic PT pathway (light blue) including C169, a water cluster, E141, and other residues. The light blue circle marks the open coordination site at Fe_d in the oxidized state, Hox. At the [4Fe–4S] cluster, C417 may receive a proton directly from the solvent *via* the regulatory PT pathway (brown).

^aDepartment of Physics, Freie Universität Berlin, 14195 Berlin, Germany.

E-mail: sven.stripp@fu-berlin

^bDepartment of Chemistry, Technische Universität Berlin, 10623 Berlin, Germany

^cFaculty of Physics, St. Petersburg State University, 198504 St. Petersburg, Russian Federation

^dFaculty of Biology and Biotechnology, Ruhr-Universität Bochum, 44801 Bochum, Germany

^eFaculty of Chemistry and Biochemistry, Ruhr-Universität Bochum, 44801 Bochum, Germany

^fFraunhofer UMSICHT, 46047 Oberhausen, Germany

^gDepartment of Chemistry, Uppsala University, 75120 Uppsala, Sweden.

E-mail: moritz.senger@kemi.uu.se

† Electronic supplementary information (ESI) available. See DOI: 10.1039/d1dt00110h



Moreover, the secondary amine of the ADT ligand serves as proton relay between the diiron site and the amino acid residues of the catalytic proton transfer pathway (Fig. 1).^{18–23} The latter includes arginine and glutamic acid residues connected by a cysteine, a serine, and a small water cluster.²⁴

The diiron site and the [4Fe–4S] cluster exist in an oxidized and reduced form each, resulting in a total of four different H-cluster species: the oxidized state, **Hox**, the 1e[−]-reduced states **Hred'** (reduced [4Fe–4S] cluster) and **Hred** (reduced diiron site) as well as the 2e[−]-reduced state, **Hsred**.^{25–32} An additional state, **Hhyd**, is comprised of a reduced [4Fe–4S] cluster and a formally over-oxidized diiron site with a terminal hydride ligand (H[−]).^{33–35} Additional states include the CO-inhibited states **Hox-CO** and **Hred'-CO** and the oxidized protonated state, **HoxH**.^{29,32} While most authors agree on the importance of **Hred'** and **Hhyd** in hydrogen turnover (Fig. 2), the protonation state, cofactor geometry, and involvement in catalysis of **Hred** and **Hsred** are under discussion.³⁶

Fig. 2 highlights that the 1e[−]-reduced H-cluster states **Hred'** and **Hred** are enriched upon coupled or sequential electron- and proton transfer (PCET or ETPT). Due to the transient nature of electron tunnelling *via* the [4Fe–4S] cluster reduction, we will only use the PCET nomenclature in the following. In previous work, we suggested that a cysteine residue coordinating the [4Fe–4S] cluster may bind a proton in **Hred'** (Fig. 1);^{31,38} however, there is no consensus regarding the nature of protonation and cofactor geometry in **Hred**. Sommer *et al.* presumed protonation of the ADT ligand (−NH₂) and a shift of the μCO ligand into a ‘semi-bridging’ position at Fe_d as seen in hydrogenase crystals grown under 10% H₂ and pressurized with 6 bar H₂.^{39,40} Ratzloff *et al.* proposed a −NH₂ geometry with a conserved μCO ligand in

Hred,⁴¹ which was supported in recent infrared studies by Birrell *et al.* and Lorent *et al.* that identified a μCO ligand for **Hred** and **Hsred** at cryogenic temperatures.^{37,42} In contrast, our infrared evaluation of **Hred** and **Hsred** at ambient temperature implied the formation of a bridging hydride species (μH) and an apical CO ligand at Fe_d.³⁰ A μH geometry was calculated to be rather unreactive.^{43–45} Therefore, such changes would exclude **Hred** and **Hsred** from the catalytic cycle (in contrast to Model 1 in Fig. 2) and favor a catalytic mechanism without the reduction of the diiron site (*i.e.*, Model 2 in Fig. 2). Sanchez *et al.* demonstrated the kinetic competence of both **Hred'** and **Hred** at ambient temperature⁴⁶ but the spectroscopic marker bands that were used to follow **Hred** in their study are nearly identical for the μCO and the μH geometry. This impedes a kinetic discrimination of these isomers.^{37,42} We presume that the cryogenic states may represent kinetically trapped intermediates.^{24,47}

The influence of bulk pH on **Hox**, **Hred**, and **Hsred** in the native [FeFe]-hydrogenase from *Chlamydomonas reinhardtii* (*CrHydA1*)^{32,39} and **Hred'** in cofactor variant *CrHydA1*^{PDT} was analysed before.^{31,48} To understand the equilibrium of **Hred'** and **Hred** in native *CrHydA1*, we now investigate the pH-dependent accumulation of both 1e[−]-reduced H-cluster states under turnover conditions. Making use of *operando* attenuated total reflection Fourier-transform infrared (ATR FTIR) spectroscopy and spectro-electrochemistry under H₂ oxidation or H₂ evolution conditions, we found consistent trends for an accumulation of **Hred'** towards alkaline pH values whereas the accumulation of **Hred** increases towards acidic pH values. This observation is explained by site-selective PCET to either the diiron site or the [4Fe–4S] cluster, guided by differences in proton affinity. Our findings are employed to distinguish catalytic from regulatory H-cluster states and inspire a molecular understanding of the pH-dependent hydrogen turnover of [FeFe]-hydrogenase.

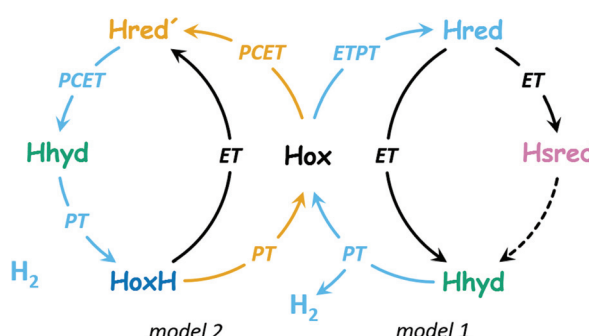


Fig. 2 Two proposals of the catalytic cycle. In H₂ evolution direction, both cycles start from **Hox**. Model 1 (right side, based on ref. 37) is characterized by ETPT to the diiron site in the 1st step (formation of **Hred**, protonation of the diiron site). This includes transient electron transfer (ET) via the [4Fe–4S] cluster and proton transfer (PT) in the formation of **Hred**. A subsequent reduction step (ET) may form **Hhyd** either directly or *via* **Hsred** by an unknown mechanism (dashed arrow). With a 2nd proton, H₂ is released and **Hox** is restored. Model 2 (left side, based on ref. 36) is characterized by PCET to the [4Fe–4S] cluster in the 1st step (formation of **Hred'**, binding of a regulatory proton at the [4Fe–4S] cluster). Subsequently, PCET to the diiron site promotes formation of **Hhyd**, and with a 3rd proton, H₂ is released and **HoxH** is formed. The latter may lose the regulatory proton to restore **Hox** or accept an electron to form **Hred'** directly.

Experimental

Protein purification and activation

All experiments involving *CrHydA1* were performed under strictly anaerobic conditions. *CrHydA1* apo-protein (wild-type and amino acid variants)^{49–51} and the synthetic mimics of the diiron site (ADT and PDT)^{19,20} were prepared as described previously. Activated *CrHydA1* was eluted in 10 mM Tris/HCl (pH 8). Sodium dithionite was avoided to prevent accumulation of **HoxH** and **Hhyd** at low pH values.^{32,34} Each sample was diluted 1 : 1 (~0.5 mM *CrHydA1*) with mixed buffer containing 50 mM Tris, MES, and PIPPS to adjust the desired pH value.

ATR FTIR spectroscopy

The FTIR spectrometer (Tensor27, Bruker) was equipped with a triple-reflection ZnSe/Si crystal ATR cell (Smith Detection) and placed in an anaerobic chamber. Infrared spectra were recorded with 80 kHz scanning velocity at a spectral resolution of 2 cm^{−1} (MCT detection). Under these conditions, the time-resolution of data acquisition is in the range of seconds (*i.e.*, five interferometer scans in forward/backward direction). ATR



FTIR measurements were performed at 25 °C and on hydrogenase films derived by controlled dehydration and rehydration of 1 μ L protein sample as reported earlier.²⁹

The anaerobically purified and activated [FeFe]-hydrogenase typically contained the H-cluster in various states. **Hox** was enriched in the film under a constant stream of N₂ for 30–60 minutes. A constant gas stream (1.5 L min⁻¹) was adjusted with digital mass flow controllers (SmartTrak, Sierra). Then, H₂ was added to the N₂ stream *via* separate flow controllers and passed through a wash bottle containing 150 mL mixed buffer (0.1–100% at ambient pressure). The resulting aerosol was fed into a gas-tight PCTFE compartment, attached on top of the ATR crystal plate and equipped with six optional gas inlets, a manometer for pressure control, and a glass window for UV/vis irradiation.²⁹ For each H₂ concentration step, the film was equilibrated for 2.5 min to ensure a sufficiently stable composition of H-cluster states (Fig. S1†).

ATR FTIR spectro-electrochemistry

The pH-dependent reduction of CrHydA1 in the absence of H₂ was analyzed by ATR FTIR spectro-electrochemistry.^{30,31} For this, 1 μ L protein sample (diluted with 50 mM mixed buffer pH 9–5) was injected into a 9 μ m thin gold mesh on top of an ATR silicon crystal. The mesh was covered with an 8 kDa dialysis membrane to protect the film from dilution. A custom-made PCTFE electrochemical cell was attached to the ATR crystal plate and filled with 3 mL electrolyte buffer (50 mM mixed buffer pH 9–5 including 500 mM KCl as electrolyte) that was purged with N₂ throughout the whole experiment. After 60–90 minutes, the film was fully hydrated and stable. The gold mesh was connected with the working electrode, a platinum wire was used as counter electrode, and an Ag/AgCl electrode served as reference (+230 mV vs. SHE, as determined with 1 mM methyl viologen at pH 7).³¹ After complete oxidation at -100 mV vs. SHE, the potential was lowered incre-

mentally from -150 mV to -850 mV in steps of 50 mV with a fixed duration of 20 minutes for each step (Fig. S2†) until no further spectral changes were observed. Midpoint potentials were estimated from bi-sigmoidal fits. At strongly reducing potentials, smaller changes in current hinted at imperfect equilibria (Fig. S2†).

Data treatment

All absorbance spectra were derived from single channel spectra of 'reference' (ZnSe/Si) and 'sample' (ZnSe/Si + protein) in OPUS software. Then, data was exported to a home-written routine as described previously.³² In the frequency regime of the H-cluster (2150–1750 cm⁻¹), absorbance spectra were subtracted with a polynomial function simulating the low-frequency combination band of liquid water underneath the 'sharp' CO/CN⁻ bands of the H-cluster. This gave rise to background-corrected spectra as shown in Fig. S1–S3.† Reference spectra of pure redox states (Fig. 3 and Fig. S3†) allowed determining fit parameters for all observed redox states (frequency, intensity, bandwidth, and peak ratio, see Table S1†), as described earlier.³² The sum of band area (2 CN⁻ + 3 CO) for a given redox state was obtained by simulation of spectral data with a fixed set of parameters that represent the population in relation to the other redox states. This value (%) and was plotted against time illustrating how the system converges into new redox equilibria upon disturbance (*i.e.*, changes in H₂ concentration in Fig. S1† or electrochemical potential in Fig. S2†). In the final step, the population of redox states was plotted as a function of H₂ concentration or electrochemical potential.

Results

All experiments were performed with the [FeFe]-hydrogenase CrHydA1 under ambient conditions. In the first step, ATR FTIR spectroscopy and spectro-electrochemistry^{29–31} were

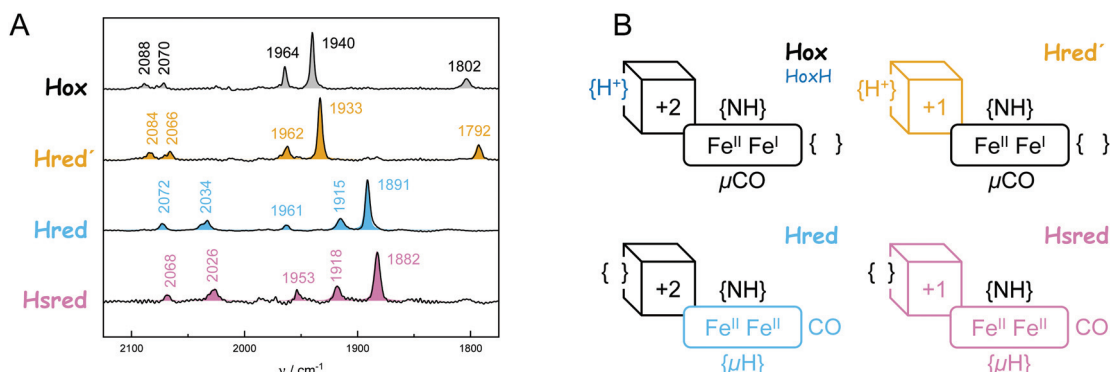


Fig. 3 Characterization of key H-cluster states. (A) Background-corrected spectra of **Hox** (grey) and **Hred'** (brown) recorded under alkaline conditions[:] (pH 9) at -300 mV vs. SHE and -600 mV vs. SHE, respectively. Additionally, the figure shows background-corrected spectra recorded either upon illumination in the presence of eosin Y and EDTA (**Hred**, light blue) or under acidic conditions (pH 5) at -800 mV vs. SHE (**Hsred**, rose). (B) Proposed H-cluster geometries. The rectangle represents the diiron site including the ADT ligand (NH), the Fe–Fe bridging ligand (μ CO, μ H), and the apical binding site of Fe_d (vacant or occupied with CO). Observed charges are formally +4 to +2. The cube represents the [4Fe–4S] cluster (charges +2 or +1). Colors hint at differences relative to **Hox** (color code: **Hox** (black), **HoxH** (dark blue), **Hred'** (brown), **Hred** (light blue), **Hsred** (rose)).

Table 1 Vibrational and electronic properties of different H-cluster states. In **Hox**–CO, vibrational coupling results in an additional IR band at 2012 cm^{-1} . In **Hred** and **Hsred** the low-frequency μCO ligand moved into a terminal position at 1961 and 1953 cm^{-1} . **Hhyd** is best described with an ‘over-oxidized’ diiron site (+4) and a terminal hydride ligand that accounts for two electrons

	$\text{CN}^-/\text{cm}^{-1}$	CO/cm^{-1}	[4Fe]	[2Fe]
Hox	2088	2070	1964	1940
Hox –CO	2092	2082	1968	1962
Hred'	2084	2066	1962	1933
Hhyd	2082	2068	1978	1960
Hred	2072	2034	1961	1915
Hsred	2068	2026	1953	1918
			1802	1891
			+2	+2
			+3	+2
			+1	+3
			+1	+4
			+2	+2
			+1	+2

employed to extract the IR signatures of all relevant redox states (Table 1 and Fig. S3†). Fig. 3A shows spectra of **Hox** and **Hred'** recorded under alkaline conditions (pH 9) at -300 mV vs. SHE and -600 mV vs. SHE, respectively. A pure spectrum of **Hred'** in native *CrHydA1* has not been reported before. Additionally, Fig. 3A shows spectra recorded either upon illumination in the presence of eosin Y and EDTA (**Hred**, see ref. 52 for the protocol) or under acidic conditions (pH 5) at -800 mV vs. SHE (**Hsred**). The overall downshift of the cofactor bands from **Hox** \rightarrow **Hred'** and **Hred** \rightarrow **Hsred** has been attributed to a reduction of the [4Fe–4S] cluster (depicted as a cubane in Fig. 3B).^{27,28} Fig. S4† emphasized that the **Hred** \rightarrow **Hsred** difference spectrum shows no signal around 1800 cm^{-1} . This highlights the lack of a μCO ligand at the reduced diiron site (depicted as a rectangle in Fig. 3B) and confirms the assignment of bands at 1961 cm^{-1} and 1953 cm^{-1} to **Hred** and **Hsred**, respectively. A detailed discussion of the IR spectrum of **Hred** can be found in ref. 47. Based on previous work,³⁰ **Hred** and **Hsred** are depicted with a terminal CO ligand and a μH ligand in Fig. 3B.

To address the pH-dependent population of H-cluster states under H_2 oxidation conditions, we investigated *CrHydA1* by ATR FTIR spectroscopy at different H_2 concentration (without external potential control). Direct proof for the hydrogenase-catalysed cleavage of H_2 came from D_2 oxidation experiment in an aqueous environment.³⁴ Moreover, H_2 oxidation induces an accumulation of reduced H-cluster states so that we were able to follow the increase and decrease of redox state populations as a function of atmospheric H_2 and time. As an example, Fig. 4A depicts a series of background-corrected ATR FTIR absorbance spectra of the H-cluster recorded after 2.5 min under 0–100% H_2 (compare Fig. S1†). We note that residual, unidentified H-cluster states may be present in the spectra. As these contributions did not interfere with the global fit analysis (*i.e.*, $\chi^2 < 10^{-4}$) we did consider them any further. Broader features in the corrected spectra stem from the ‘combination band’ of liquid water. For a spectroscopically unique identification of H-cluster states, see Fig. 3A and ESI.† Fig. 4B illustrates how increasing the H_2 concentration to 0.1% resulted in an accumulation of 1e^- -reduced states **Hred'** and **Hred**, which remained fairly stable between 0.1–3% H_2 . At higher concen-

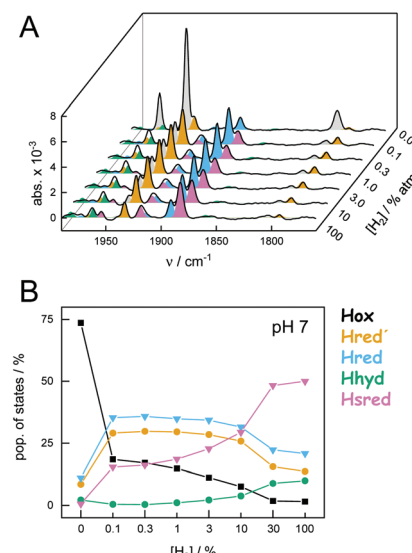


Fig. 4 Composition of H-cluster states under H_2 oxidation conditions (pH 7). All data recorded on a hydrated film of *CrHydA1* at ambient temperature and 0–100% H_2 in the gas phase. (A) Series of baseline-corrected FTIR absorbance spectra of the H-cluster obtained after 2.5 min at each step. (B) State populations as a function of $[\text{H}_2]$. Between 0.1–3% H_2 , the population of **Hred'** and **Hred** was relatively stable. **Hsred** dominated for $[\text{H}_2] > 10\%$.

trations of H_2 , the 2e^- -reduced **Hsred** state dominated the spectrum. Only minor traces of the 2e^- -reduced **Hhyd** state were observed, most likely due to the lack of sodium dithionite in the sample (see Experimental section).³⁴

Analogous to the experiment shown in Fig. 4, six individual *CrHydA1* protein films between pH 10–5 were analyzed (Fig. 5). Largely independent of pH, the oxidized state **Hox** was the most prominent species in the absence of H_2 while **Hsred** dominated the spectrum for $[\text{H}_2] > 10\%$ (Fig. S5†). The steady-state population of **Hred'** and **Hred** is plotted as a function of $[\text{H}_2]$ and at different pH values in Fig. 5AB. Here, we observed diverging trends for the accumulation of the 1e^- -reduced states: **Hred** dominated at acidic conditions whereas **Hred'** was promoted under alkaline pH values. Fig. 5C depicts the accumulation of **Hred'** and **Hred** at 3% H_2 as a function of pH, which clearly illustrates this trend. At low pH and $[\text{H}_2] > 10\%$, an increasing accumulation of **Hhyd** was observed, which may explain the mild suppression of **Hsred** that was otherwise expected to follow the same pH dependence as **Hred** (Fig. S5†). Upon removal of H_2 from the gas stream, the 2e^- -reduced states **Hhyd** and **Hsred** converted transiently into the 1e^- -reduced states **Hred'** and **Hred**, indicating intermolecular electron transfer in the dense films,³² before the equilibrium shifted back towards **Hox** upon auto-oxidation.¹⁷ The diverging pH dependence of **Hred'** and **Hred** was found to be well conserved in this transient increase, emphasizing the robustness of all observed trends (Fig. S6†).

The simultaneous presence of **Hred'** and **Hred** complicates unique conclusions regarding the mechanism of H-cluster protonation. Therefore, additional experiments were performed.



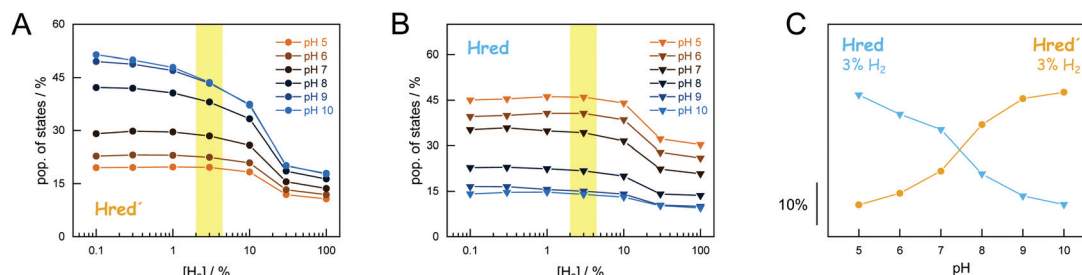


Fig. 5 Accumulation of **Hred'** and **Hred** as a function of H_2 and pH. Population of **Hred'** (panel A) and **Hred** (panel B) for six different pH values (pH 10–5) under 0.1–100% H_2 . Plotting the population of **Hred'** and **Hred** at 3% H_2 (yellow mark-up) against pH clearly illustrates the opposing pH dependency (panel C). For $[\text{H}_2] > 10\%$, **Hsred** and **Hhyd** are accumulated.

First, we probed the pH dependence of H_2 oxidation with *CrHydA1*^{PDT}. This cofactor variant lacks the secondary amine of the native ADT ligand (Fig. 1) and allows analysing the reduction of the [4Fe–4S] cluster (*i.e.*, the **Hox** → **Hred'** transition) independent from redox chemistry at the diiron site.^{28,31} Fig. S7† shows that the H_2 oxidation activity of *CrHydA1*^{PDT} increases between pH 10–8. While this cannot be explained by the stoichiometry of the catalysed reaction, our results support PCET chemistry at the [4Fe–4S] cluster.³¹ Earlier, the influence of cysteinyl ligand C417 on the catalytic properties of *CrHydA1* has been addressed by site-directed mutagenesis.^{50,51} Now, we analyzed three cysteine variants to compare the composition of H-cluster states under H_2 oxidation conditions (Fig. S8†). We made the following observations. (i) C417S behaved much like wild-type *CrHydA1* but showed a reduced percentage of **Hred'** under H_2 . (ii) Due to electron withdrawal from the [4Fe–4S] cluster by the imidazole ligand, C417H was reported with a less negative redox potential than wild-type *CrHydA1*.⁵¹ In agreement with earlier observations C417H adopted **Hred'** as a resting state, reflecting the lack of H_2 evolution activity of *CrHydA1* C417H.⁵¹

In the presence of H_2 , the variant converted into **Hsred** (at pH 8) or **Hhyd** (pH 4) with no detectable traces of **Hred**. In the absence of H_2 , low pH conditions resulted in an accumulation of **Hred'H**. (iii) The spectral behavior of C417D was surprisingly similar to C417H, indicative of electron withdrawal. We speculate that this may be due to hydrogen-bonding between the aspartic acid side chain and the [4Fe–4S] cluster. In variance to the histidine variant, C417D slowly converted into **Hox** (pH 8) or **HoxH** (pH 4), reflecting the low but significant H_2 evolution activity of *CrHydA1* C417D.⁵⁰

Overall, our data demonstrate how the equilibrium of redox states is affected by cluster ligation, proton concentration (pH), and the percentage of H_2 in the gas phase. Under H_2 oxidation conditions, virtually all H-cluster species were present at every step of the experiment, impeding an individual analysis of states. Thus, we investigated the pH-dependent population of redox states in *CrHydA1* under H_2 evolution conditions by injecting electrons into the systems in the absence of H_2 . We employed ATR FTIR spectro-electrochemistry to follow the evolution of state populations as a function of electrochemical potential. In contrast to conventional, Moss-

type⁵³ transmission cells, the ATR FTIR spectro-electrochemistry approach allowed H_2 to be released from the protein-modified working electrode hence precluding product oxidation or product inhibition. Fig. 6 depicts how the oxidized states **Hox** and **Hox-CO** were lost at reductive potentials, followed by accumulation of the 1e^- -reduced states **Hred'** and **Hred**. Upon further reduction, accumulation of **Hsred** was observed; however, in contrast to the experiments performed under H_2 oxidation conditions (Fig. 4), **Hhyd** was not observed.

Analogous to the experiment shown in Fig. 6, nine individual protein films between pH 9–5 were analyzed (Fig. 7). The maximal population of H-cluster states as a function of poten-

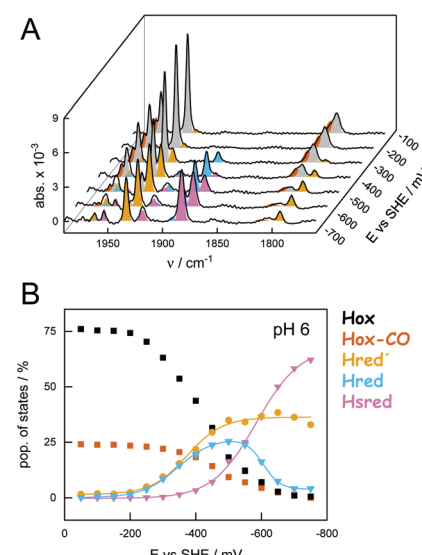


Fig. 6 Composition of H-cluster states under H_2 evolution conditions (pH 6). Exemplary data recorded on a hydrated film of *CrHydA1* between -50 and -750 mV vs. SHE and constant N_2 purging. (A) Series of baseline-corrected ATR FTIR absorbance spectra of the H-cluster obtained after 20 min at each increment of 50 mV (steady-state conditions). (B) State populations as a function of electrochemical potential. Sigmoidal fits allowed approximating the following midpoint potentials (vs. SHE): **Hox** → **Hred'** -375 mV; **Hox** → **Hred** -345 mV; **Hred** → **Hsred** -585 mV (a second fit component at -605 mV may account for **Hred'** → **Hsred**).



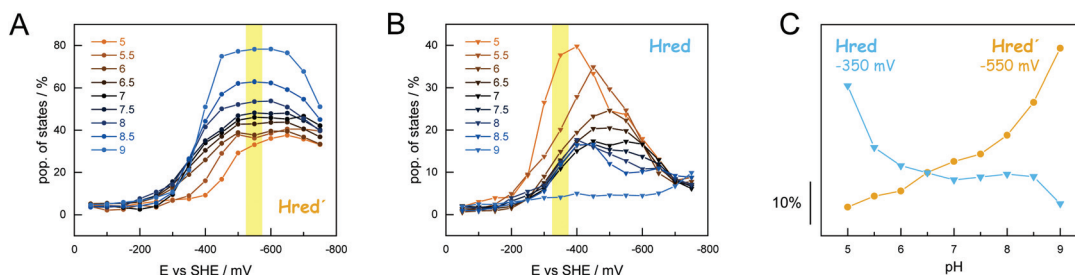


Fig. 7 Accumulation of **Hred'** and **Hred** as a function of electrochemical potential and pH. Population of **Hred'** (panel A) and **Hred** (panel B) for nine different pH values (pH 9–5) between -50 and -750 mV vs. SHE. The opposite pH dependence is clearly illustrated plotting the population of **Hred'** (-550 mV vs. SHE) and **Hred** (-350 mV vs. SHE) as function of pH in panel C (the yellow mark-up highlights the respective potentials).

tial and pH value was used as the main observable. This approach allowed analyzing the $1e^-$ - and $2e^-$ -reduced states separately, which was not possible under H_2 oxidation conditions (Fig. 5). The oxidized state **Hox** was the most prominent species at potentials more positive than -350 mV vs. SHE, largely independent of pH (*i.e.*, in the absence of dithionite³²). The accumulation of **Hsred** was found to be affected by pH more drastically, with a higher population at acidic pH values that reflects the lack of **Hhyd** in the experiment (Fig. S9†). Overall, we observed a mean midpoint potential around -650 mV vs. SHE for **Hsred**, which leaves a potential window of ~ 300 mV to analyze the accumulation of the $1e^-$ -reduced states.

In Fig. 7AB the steady-state population of **Hred'** and **Hred** is plotted as a function of potential and at different pH values. Like what has been observed under H_2 oxidizing conditions, **Hred** dominated under acidic conditions whereas **Hred'** was promoted at alkaline pH values. The population of states varies from 30–80% (-550 mV vs. SHE, **Hred'**) and 40–5% (-350 mV vs. SHE, **Hred**) for increasing pH values. Fig. 7C depicts the accumulation of **Hred'** and **Hred** as a function of pH. This trend is strictly conserved in the aforementioned potential window (Fig. S9†) and facilitated an estimation of apparent proton affinities for the accumulation of **Hred'** and **Hred**. Moreover, the Pourbaix diagram in Fig. S9† highlights the decrease in electrochemical driving force for **Hox** \rightarrow **Hred'** between pH 9–8 and **Hox** \rightarrow **Hred** between pH 6–5. Interestingly, no pronounced pH dependency is observed around pH 7, which may reflect the concomitant formation of **Hred'** and **Hred**.

Discussion

We analyzed the [FeFe]-hydrogenase HYDA1 from *Chlamydomonas reinhardtii* by ATR FTIR spectroscopy and spectro-electrochemistry under ambient conditions. We addressed the pH-dependent accumulation of various H-cluster states. Varying the sample pH under H_2 oxidation and H_2 evolution conditions established consistent trends for the accumulation of $1e^-$ -reduced H-cluster states: we observed enrichment of **Hred** under acidic conditions whereas **Hred'**

prevailed at alkaline conditions. Our data on cofactor and amino acid variants highlight the importance of the [4Fe–4S] cluster for catalysis and the equilibrium of redox species.

In earlier work, we identified the pH dependence of **Hred'** formed upon reduction of the [4Fe–4S] cluster and protonation of a nearby cysteine, C417 in *CrHydA1*.³¹ Moreover, the **Hred'** state is involved in the steady-state accumulation of **HoxH**,³² which proceeds under reducing conditions exclusively and represents the starting state for an enrichment of **Hhyd** in the presence of H_2 .^{34,54} While these data indicate PCET to the [4Fe–4S] cluster and emphasize the importance of redox chemistry adjacent to the diiron site, an understanding of the pH dependence of **Hred'** and **Hred** with respect to hydrogen turnover is yet to be accomplished. Due to the simultaneous presence of various reduced H-cluster states under H_2 (including **Hhyd** and **Hsred**), unraveling the PCET chemistry of **Hred'** and **Hred** was found to be challenging.³⁹ To this end, ATR FTIR spectro-electrochemistry facilitated analyzing the population of $1e^-$ - and $2e^-$ -reduced H-cluster states individually. The accumulation of **Hred** at acidic pH values and mildly reducing conditions (*e.g.*, -350 mV vs. SHE) suggests a slightly acidic pK_a , in agreement with the involvement of glutamic acid residues as ‘bottle neck’ in the catalytic PT pathway.²¹ In contrast, our data for the population of **Hred'** at more reducing potentials (*e.g.*, -550 mV vs. SHE) hints at a pK_a in the alkaline, which reflects the greater ease of proton transfer to the [4Fe–4S] cluster *via* bulk solvent^{32,36} and is in excellent agreement with the formal pK_a of 8.1 for a cysteine sidechain. This observation is evidence for the pH dependence of **Hred'** in native [FeFe]-hydrogenase, in particular because the **Hred** state does not show dedicated pH dependence in this pH window. Surprisingly, Rodríguez-Macia *et al.* found the redox potential of the [4Fe–4S] cluster in *CrHydA1*^{PDT} to be independent from bulk pH.⁴⁸ The reasons for this discrepancy are unclear. In our hands, present and previous data^{31,38} support PCET in the formation of **Hred'**. We propose to distinguish a catalytic PT pathway to the diiron site from a regulatory pathway to the [4Fe–4S] cluster as a common feature of [FeFe]-hydrogenases.

Both *in vivo* and *in vitro*, the pH dependence of H_2 evolution of [FeFe]-hydrogenase shows a bell-shaped distribution with a maximal activity around neutral or mildly alkaline pH values.^{55–58} This has recently been confirmed by bulk electro-



chemistry.⁵⁹ While the increase in H₂ evolution activity between pH 9–7 can be attributed to rising proton concentration, our data on *CrHydA1* now allows correlating the activity decrease between pH 7–5 to the formation of **Hred**, which clearly dominated over **Hred'** at acidic pH values. Although our data does not report on enzymatic activity directly, this behavior is in agreement with **Hred** and **Hsred** as 'H₂-inhibited' states⁶⁰ that bind a bridging hydride at the diiron site³⁰ and have been shown to play a key role in sensory [FeFe]-hydrogenases.^{61–63} The ligand flip required to form a reactive terminal hydride geometry disfavors fast catalysis.^{43–45} The present data support the theory that reduction and site-selective protonation at the [4Fe–4S] cluster adjusts the redox potential of the H-cluster to stabilize a reactive geometry necessary for efficient hydrogen catalysis.³⁶ We suggest that similar concepts may give rise to a novel generation of biomimetic hydrogen catalysts.

Conflicts of interest

There are no conflicts to declare.

Acknowledgements

We thank all reviewers for the critical feedback. Konstantin was supported by the Einstein Foundation Berlin. The research stay of Iuliiia was funded by G-RISC (Grant No. P-2016b-28). We thank the Studienstiftung des Deutschen Volkes for a Kekulé Mobility Fellowship (to Leonie) and a PhD fellowship (to Florian). Ulf acknowledges funding by the DFG (under Germanys' Excellence Strategy – EXC 2033–390677874) and the Fraunhofer Internal Programs (Grant No. ATTRACT 097-602175). Thomas acknowledges financial support from the Volkswagen Stiftung (Grant No. Az 93412) and the DFG (under Germanys' Excellence Strategy – EXC 2033–390677874 and GRK 2341 Microbial Substrate Conversion). The European Union's Horizon 2020 research and innovation program is gratefully acknowledged for funding to Moritz (Marie Skłodowska-Curie Grant No. 897555). Sven is funded by the German Research Foundation (DFG) within the framework of SPP 1927 priority program "Iron-Sulfur for Life" (Grant No. STR1554/5-1).

References

- 1 W. Lubitz, H. Ogata, O. Rüdiger and E. Reijerse, Hydrogenases, *Chem. Rev.*, 2014, **114**(8), 4081–4148, DOI: 10.1021/cr4005814.
- 2 J. W. Peters, G. J. Schut, E. S. Boyd, D. W. Mulder, E. M. Shepard, J. B. Broderick, P. W. King and M. W. Adams, [FeFe]- and [NiFe]-Hydrogenase Diversity, Mechanism, and Maturation, *Biochim. Biophys. Acta*, 2015, **1853**(6), 1350–1369, DOI: 10.1016/j.bbamcr.2014.11.021.
- 3 H. Land, M. Senger, G. Berggren and S. T. Stripp, Current State of [FeFe]-Hydrogenase Research - Biodiversity and Spectroscopic Investigations, *ACS Catal.*, 2020, **10**, 7069–7086, DOI: 10.1021/acscatal.0c01614.
- 4 J. T. Kleinhaus, F. Wittkamp, S. Yadav and D. Siegmund, ; Apfel, U.-P. [FeFe]-Hydrogenases: Maturation and Reactivity of Enzymatic Systems and Overview of Biomimetic Models, *Chem. Soc. Rev.*, 2021, DOI: 10.1039/d0cs01089h, Advance article.
- 5 C. Greening, A. Biswas, C. R. Carere, C. J. Jackson, M. C. Taylor, M. B. Stott, G. M. Cook and S. E. Morales, Genomic and Metagenomic Surveys of Hydrogenase Distribution Indicate H₂ Is a Widely Utilised Energy Source for Microbial Growth and Survival, *ISME J.*, 2016, **10**(3), 761–777, DOI: 10.1038/ismej.2015.153.
- 6 A. Hemschemeier and T. Happe, Alternative Photosynthetic Electron Transport Pathways during Anaerobiosis in the Green Alga *Chlamydomonas Reinhardtii*, *Biochim. Biophys. Acta, Bioenerg.*, 2011, **1807**(8), 919–926, DOI: 10.1016/j.bbabi.2011.02.010.
- 7 J. W. Peters, W. N. Lanzilotta, B. J. Lemon and L. C. Seefeldt, X-Ray, Crystal Structure of the Fe-Only Hydrogenase (CpI) from *Clostridium Pasteurianum* to 1.8 Angstrom Resolution, *Science*, 1998, **282**(5395), 1853–1858, DOI: 10.1126/science.282.5395.1853.
- 8 Y. Nicolet, C. Piras, P. Legrand, C. E. Hatchikian and J. C. Fontecilla-Camps, *Desulfovibrio Desulfuricans* Iron Hydrogenase: The Structure Shows Unusual Coordination to an Active Site Fe Binuclear Center, *Structure*, 1999, **7**(1), 13–23, DOI: 10.1016/S0969-2126(99)80005-7.
- 9 J. Cohen, K. Kim, P. W. King, M. Seibert and K. Schulten, Finding Gas Diffusion Pathways in Proteins: Application to O₂ and H₂ Transport in CpI [FeFe]-Hydrogenase and the Role of Packing Defects, *Structure*, 2005, **13**(9), 1321–1329, DOI: 10.1016/j.str.2005.05.013.
- 10 P. Liebgott, F. Leroux, B. Burlat and S. Dementin, Relating Diffusion along the Substrate Tunnel and Oxygen Sensitivity in Hydrogenase, *Nat. Chem. Biol.*, 2009, **6**, 63–70, DOI: 10.1038/nchembio.276.
- 11 D. W. Mulder, E. M. Shepard, J. E. Meuser, N. Joshi, P. W. King, M. C. Posewitz, J. B. Broderick and J. W. Peters, Insights into [FeFe]-Hydrogenase Structure, Mechanism, and Maturation, *Structure*, 2011, **19**(8), 1038–1052, DOI: 10.1016/j.str.2011.06.008.
- 12 T. Lautier, P. Ezanno, C. Baffert, V. Fourmond, L. Cournac, J. C. Fontecilla-Camps, P. Soucaille, P. Bertrand, I. Meynial-Salles and C. Léger, The Quest for a Functional Substrate Access Tunnel in FeFe Hydrogenase, *Faraday Discuss.*, 2011, **148**, 385, DOI: 10.1039/c004099c.
- 13 M. Winkler, J. Esselborn and T. Happe, Molecular Basis of [FeFe]-Hydrogenase Function: An Insight into the Complex Interplay between Protein and Catalytic Cofactor, *Biochim. Biophys. Acta*, 2013, **1827**(8–9), 974–985, DOI: 10.1016/j.bbabi.2013.03.004.
- 14 P. Knörzer, A. Silakov, C. E. Foster, F. A. Armstrong, W. Lubitz and T. Happe, Importance of the Protein



Framework for Catalytic Activity of [FeFe]-Hydrogenases, *J. Biol. Chem.*, 2012, **287**(2), 1489–1499, DOI: 10.1074/jbc.M111.305797.

15 J. F. Siebel, A. Adamska-Venkatesh, K. Weber, S. Rumpel, E. Reijerse and W. Lubitz, Hybrid [FeFe]-Hydrogenases with Modified Active Sites Show Remarkable Residual Enzymatic Activity, *Biochemistry*, 2015, **54**(7), 1474–1483, DOI: 10.1021/bi501391d.

16 O. Lampret, A. Adamska-Venkatesh, H. Konegger, F. Wittkamp, U.-P. Apfel, E. J. Reijerse, W. Lubitz, O. Rüdiger, T. Happe and M. Winkler, Interplay between CN Ligands and the Secondary Coordination Sphere of the H-Cluster in [FeFe]-Hydrogenases, *J. Am. Chem. Soc.*, 2017, **139**(50), 18222–18230, DOI: 10.1021/jacs.7b08735.

17 J. Duan, S. Mebs, K. Laun, F. Wittkamp, J. Heberle, E. Hofmann, U.-P. Apfel, M. Winkler, M. Senger, M. Haumann and S. T. Stripp, Geometry of the Catalytic Active Site in [FeFe]-Hydrogenase Is Determined by Hydrogen Bonding and Proton Transfer, *ACS Catal.*, 2019, **9**(10), 9140–9149, DOI: 10.1021/acscatal.9b02203.

18 A. Silakov, B. Wenk, E. Reijerse and W. Lubitz, 14N HYSCORE Investigation of the H-Cluster of [FeFe] Hydrogenase: Evidence for a Nitrogen in the Dithiol Bridge, *Phys. Chem. Chem. Phys.*, 2009, **11**(31), 6553–6554, DOI: 10.1039/b913085n.

19 G. Berggren, A. Adamska-Venkatesh, C. Lambertz, T. R. Simmons, J. Esselborn, M. Atta, S. Gambarelli, J.-M. Mouesa, E. J. Reijerse, W. Lubitz, T. Happe, V. Artero and M. Fontecave, Biomimetic Assembly and Activation of [FeFe]-Hydrogenases, *Nature*, 2013, **499**(7456), 66–69, DOI: 10.1038/nature12239.

20 J. Esselborn, C. Lambertz, A. Adamska-Venkatesh, T. Simmons, G. Berggren, J. Noth, J. F. Siebel, A. Hemschemeier, V. Artero, E. Reijerse, M. Fontecave, W. Lubitz and T. Happe, Spontaneous Activation of [FeFe]-Hydrogenases by an Inorganic [2Fe] Active Site Mimic, *Nat. Chem. Biol.*, 2013, **9**, 607–609, DOI: 10.1038/nchembio.1311.

21 J. Duan, M. Senger, J. Esselborn, V. Engelbrecht, F. Wittkamp, U.-P. Apfel, E. Hofmann, S. T. Stripp, T. Happe and M. Winkler, Crystallographic and Spectroscopic Assignment of the Proton Transfer Pathway in [FeFe]-Hydrogenases, *Nat. Commun.*, 2018, **9**, 4726, DOI: 10.1038/s41467-018-07140-x.

22 M. Senger, V. Eichmann, K. Laun, J. Duan, F. Wittkamp, G. Knör, U.-P. Apfel, T. Happe, M. Winkler, J. Heberle and S. T. Stripp, How [FeFe]-Hydrogenase Facilitates Bidirectional Proton Transfer, *J. Am. Chem. Soc.*, 2019, **141**(43), 17394–17403, DOI: 10.1021/jacs.9b09225.

23 O. Lampret, J. Duan, E. Hofmann, M. Winkler, F. A. Armstrong and T. Happe, The Roles of Long-Range Proton-Coupled Electron Transfer in the Directionality and Efficiency of [FeFe]-Hydrogenases, *Proc. Natl. Acad. Sci. USA*, 2020, **117**(34), 20520–20529, DOI: 10.1073/pnas.2007090117.

24 H. Tai, S. Hirota and S. T. Stripp, Proton Transfer Mechanisms in Bimetallic Hydrogenases, *Acc. Chem. Res.*, 2021, **54**, 232–241, DOI: 10.1021/acs.accounts.0c00651.

25 A. L. De Lacey, C. Stadler, C. Cavazza, E. C. Hatchikian and V. M. Fernandez, FTIR Characterization of the Active Site of the Fe-Hydrogenase from *Desulfovibrio Desulfuricans*, *J. Am. Chem. Soc.*, 2000, **122**(45), 11232–11233, DOI: 10.1021/ja002441o.

26 W. Roseboom, A. L. De Lacey, V. M. Fernandez, E. C. Hatchikian and S. P. J. Albracht, The Active Site of the [FeFe]-Hydrogenase from *Desulfovibrio Desulfuricans*. II. Redox Properties, Light Sensitivity and CO-Ligand Exchange as Observed by Infrared Spectroscopy, *J. Biol. Inorg. Chem.*, 2006, **11**(1), 102–118, DOI: 10.1007/s00775-005-0040-2.

27 A. Adamska-Venkatesh, A. Silakov, C. Lambertz, O. Rüdiger, T. Happe, E. Reijerse and W. Lubitz, Identification and Characterization of the “Super-Reduced” State of the H-Cluster in [FeFe] Hydrogenase: A New Building Block for the Catalytic Cycle?, *Angew. Chem., Int. Ed.*, 2012, **51**(46), 11458–11462, DOI: 10.1002/anie.201204800.

28 A. Adamska-Venkatesh, D. Krawietz, J. F. Siebel, K. Weber, T. Happe, E. Reijerse and W. Lubitz, New Redox States Observed in [FeFe] Hydrogenases Reveal Redox Coupling within the H-Cluster, *J. Am. Chem. Soc.*, 2014, **136**(32), 11339–11346, DOI: 10.1021/jacs.5a03390c.

29 M. Senger, S. Mebs, J. Duan, F. Wittkamp, U.-P. Apfel, J. Heberle, M. Haumann and S. T. Stripp, Stepwise Isotope Editing of [FeFe]-Hydrogenases Exposes Cofactor Dynamics, *Proc. Natl. Acad. Sci. USA*, 2016, **113**(30), 8454–8459, DOI: 10.1073/pnas.1606178113.

30 S. Mebs, M. Senger, J. Duan, F. Wittkamp, U.-P. Apfel, T. Happe, M. Winkler, S. T. Stripp and M. Haumann, Bridging Hydride at Reduced H-Cluster Species in [FeFe]-Hydrogenases Revealed by Infrared Spectroscopy, Isotope Editing, and Quantum Chemistry, *J. Am. Chem. Soc.*, 2017, **139**(35), 12157–12160, DOI: 10.1021/jacs.7b07548.

31 M. Senger, K. Laun, F. Wittkamp, J. Duan, M. Haumann, T. Happe, M. Winkler, U.-P. Apfel and S. T. Stripp, Proton-Coupled Reduction of the Catalytic [4Fe-4S] Cluster in [FeFe]-Hydrogenases, *Angew. Chem., Int. Ed.*, 2017, **56**(52), 16503–16506, DOI: 10.1002/anie.201709910.

32 M. Senger, S. Mebs, J. Duan, O. Shulenina, K. Laun, L. Kertess, F. Wittkamp, U.-P. Apfel, T. Happe, M. Winkler, M. Haumann and S. T. Stripp, Protonation/Reduction Dynamics at the [4Fe-4S] Cluster of the Hydrogen-Forming Cofactor in [FeFe]-Hydrogenases, *Phys. Chem. Chem. Phys.*, 2018, **20**(5), 3128–3140, DOI: 10.1039/C7CP04757F.

33 D. W. Mulder, Y. Guo, M. W. Ratzloff and P. W. King, Identification of a Catalytic Iron-Hydride at the H-Cluster of [FeFe]-Hydrogenase, *J. Am. Chem. Soc.*, 2016, **139**(1), 83–86, DOI: 10.1021/jacs.6b11409.

34 M. Winkler, M. Senger, J. Duan, J. Esselborn, F. Wittkamp, E. Hofmann, U.-P. Apfel, S. T. Stripp and T. Happe, Accumulating the Hydride State in the Catalytic Cycle of [FeFe]-Hydrogenases, *Nat. Commun.*, 2017, **8**(16115), 1–7, DOI: 10.1038/ncomms16115.

35 E. J. Reijerse, C. C. Pham, V. Pelmenschikov, R. Gilbert-wilson, A. Adamska-Venkatesh, J. F. Siebel, L. B. Gee,



Y. Yoda, K. Tamasaku, W. Lubitz, T. B. Rauchfuss and S. P. Cramer, Direct Observation of an Iron-Bound Terminal Hydride in [FeFe]-Hydrogenase by Nuclear Resonance Vibrational Spectroscopy, *J. Am. Chem. Soc.*, 2017, **139**(12), 4306–4309, DOI: 10.1021/jacs.7b00686.

36 M. Haumann and S. T. Stripp, The Molecular Proceedings of Biological Hydrogen Turnover, *Acc. Chem. Res.*, 2018, **51**(8), 1755–1763, DOI: 10.1021/acs.accounts.8b00109.

37 C. Lorent, S. Katz, J. Duan, C. Julia Kulka, G. Caserta, C. Teutloff, S. Yadav, U.-P. Apfel, M. Winkler, T. Happe, M. Horch and I. Zebger, Shedding Light on Proton and Electron Dynamics in [FeFe] Hydrogenases, *J. Am. Chem. Soc.*, 2020, **142**(12), 5493–5497, DOI: 10.1021/jacs.9b13075.

38 K. Laun, S. Mebs, J. Duan, F. Wittkamp, U.-P. Apfel, T. Happe, M. Winkler, M. Haumann and S. T. Stripp, Spectroscopical Investigations on the Redox Chemistry of [FeFe]-Hydrogenases in the Presence of Carbon Monoxide, *Molecules*, 2018, **23**(7), 1669, DOI: 10.3390/molecules23071669.

39 C. Sommer, A. Adamska-Venkatesh, K. Pawlak, J. A. Birrell, O. Rüdiger, E. J. Reijerse and W. Lubitz, Proton Coupled Electronic Rearrangement within the H-Cluster as an Essential Step in the Catalytic Cycle of [FeFe] Hydrogenases, *J. Am. Chem. Soc.*, 2017, **139**(4), 1440–1443, DOI: 10.1021/jacs.6b12636.

40 Y. Nicolet, A. L. De Lacey, X. Vernède, V. M. Fernandez, E. C. Hatchikian and J. C. Fontecilla-Camps, Crystallographic and FTIR Spectroscopic Evidence of Changes in Fe Coordination upon Reduction of the Active Site of the Fe-Only Hydrogenase from *Desulfovibrio Desulfuricans*, *J. Am. Chem. Soc.*, 2001, **123**(8), 1596–1601, DOI: 10.1021/ja0020963.

41 M. W. Ratzloff, J. H. Artz, D. W. Mulder, R. T. Collins, T. E. Furtak and P. W. King, CO-Bridged, H-Cluster Intermediates in the Catalytic Mechanism of [FeFe]-Hydrogenase CaI, *J. Am. Chem. Soc.*, 2018, **140**(24), 7623–7628, DOI: 10.1021/jacs.8b03072.

42 J. A. Birrell, V. Pelmenschikov, N. Mishra, H. Wang, Y. Yoda, T. B. Rauchfuss, S. P. Cramer, W. Lubitz and S. Debeer, Spectroscopic and Computational Evidence That [FeFe] Hydrogenases Operate Exclusively with CO-Bridged Intermediates, *J. Am. Chem. Soc.*, 2020, **142**(1), 222–232, DOI: 10.1021/jacs.9b09745.

43 G. Filippi, F. Arrigoni, L. Bertini, L. De Gioia and G. Zampella, DFT Dissection of the Reduction Step in H₂ Catalytic Production by [FeFe]-Hydrogenase-Inspired Models: Can the Bridging Hydride Become More Reactive Than the Terminal Isomer?, *Inorg. Chem.*, 2015, **54**(19), 9529–9542, DOI: 10.1021/acs.inorgchem.5b01495.

44 C. Greco, M. Bruschi, L. Gioia and U. De; Ryde, A QM/MM Investigation of the Activation and Catalytic Mechanism of Fe-Only Hydrogenases, *Inorg. Chem.*, 2007, **46**(15), 5911–5921, DOI: 10.1021/ic062320a.

45 M. Bruschi, P. Fantucci and L. De Gioia, Density Functional Theory Investigation of the Active Site of Fe-Hydrogenases. Systematic Study of the Effects of Redox State and Ligands Hardness on Structural and Electronic Properties of Complexes Related to the [2Fe](H) Subcluster, *Inorg. Chem.*, 2004, **43**(12), 3733–3741, DOI: 10.1021/ic035326y.

46 M. L. K. Sanchez, C. Sommer, E. Reijerse, J. A. Birrell, W. Lubitz and R. B. Dyer, Investigating the Kinetic Competency of CrHydA1 [FeFe] Hydrogenase Intermediate States via Time-Resolved Infrared Spectroscopy, *J. Am. Chem. Soc.*, 2019, **141**(40), 16064–16070, DOI: 10.1021/jacs.9b08348.

47 S. T. Stripp, S. Mebs and M. Haumann, Temperature Dependence of Structural Dynamics at the Catalytic Cofactor of [FeFe]-Hydrogenase, *Inorg. Chem.*, 2020, **59**(22), 16474–16488, DOI: 10.1021/acs.inorgchem.0c02316.

48 P. Rodríguez-Maciá, N. Breuer, S. DeBeer and J. A. Birrell, Insight into the Redox Behavior of the [4Fe-4S] Subcluster in [FeFe] Hydrogenases, *ACS Catal.*, 2020, **10**, 13084–13095, DOI: 10.1021/acscatal.0c02771.

49 J. M. Kuchenreuther, S. J. George, C. S. Grady-Smith, S. P. Cramer and J. R. Swartz, Cell-Free H-Cluster Synthesis and [FeFe] Hydrogenase Activation: All Five CO and CN[−] Ligands Derive from Tyrosine, *PLoS One*, 2011, **6**(5), e20346, DOI: 10.1371/journal.pone.0020346.

50 L. Kertess, A. Adamska-Venkatesh, P. Rodríguez-Maciá, O. Rüdiger, W. Lubitz and T. Happe, Influence of the [4Fe-4S] Cluster Coordinating Cysteines on Active Site Maturation and Catalytic Properties of *C. Reinhardtii* [FeFe]-Hydrogenase, *Chem. Sci.*, 2017, **8**(12), 8127–8137, DOI: 10.1039/c7sc0344j.

51 P. Rodríguez-Maciá, L. Kertess, J. Burnik, J. A. Birrell, E. Hofmann, W. Lubitz, T. Happe and O. Rüdiger, His-Ligation to the [4Fe-4S] Subcluster Tunes the Catalytic Bias of [FeFe] Hydrogenase, *J. Am. Chem. Soc.*, 2019, **141**(1), 472–481, DOI: 10.1021/jacs.8b11149.

52 M. Senger, V. Eichmann, K. Laun, J. Duan, F. Wittkamp, G. Knör, U.-P. Apfel, T. Happe, M. Winkler, J. Heberle and S. T. Stripp, How [FeFe]-Hydrogenase Facilitates Bidirectional Proton Transfer, *J. Am. Chem. Soc.*, 2019, **141**(43), DOI: 10.1021/jacs.9b09225.

53 D. Moss, E. Nabedryk, J. Breton and W. Mäntele, Redox-Linked Conformational Changes in Proteins Detected by a Combination of Infrared Spectroscopy and Protein Electrochemistry. Evaluation of the Technique with Cytochrome C, *Eur. J. Biochem.*, 1990, **187**(3), 565–572, DOI: 10.1111/j.1432-1033.1990.tb15338.x.

54 L. Mészáros, P. Ceccaldi, M. Lorenzi, H. J. Redman, E. Pfitzner, J. Heberle, M. Senger, S. T. Stripp and G. Berggren, Spectroscopic Investigations under Whole Cell Conditions Provide New Insight into the Metal Hydride Chemistry of [FeFe]-Hydrogenase, *Chem. Sci.*, 2020, **11**(18), 4608–4617, DOI: 10.1039/d0sc00512f.

55 F. P. Healey, The Mechanism of Hydrogen Evolution by *Chlamydomonas Moewusii*, *Plant Physiol.*, 1970, **45**(2), 153–159, DOI: 10.1104/pp.45.2.153.

56 U. Klein and A. Betz, Induced Protein Synthesis during the Adaptation to H₂ Production in *Chlamydomonas Moewusii*, *Physiol. Plant.*, 1978, **42**(1), 1–4, DOI: 10.1111/j.1399-3054.1978.tb01529.x.



57 P. Roessler and S. Lien, Anionic Modulation of the Catalytic Activity of Hydrogenase from *Chlamydomonas Reinhardtii*, *Arch. Biochem. Biophys.*, 1982, **213**(1), 37–44, DOI: 10.1016/0003-9861(82)90436-2.

58 T. Happe and J. D. Naber, Isolation, Characterization and N-terminal Amino Acid Sequence of Hydrogenase from the Green Alga *Chlamydomonas Reinhardtii*, *Eur. J. Biochem.*, 1993, **214**(2), 475–481, DOI: 10.1111/j.1432-1033.1993.tb17944.x.

59 J. C. Ruth, R. D. Milton, W. Gu and A. M. Spormann, Enhanced Electrosynthetic Hydrogen Evolution by Hydrogenases Embedded in a Redox-Active Hydrogel, *Chem. – Eur. J.*, 2020, **26**(32), 7323–7329, DOI: 10.1002/chem.202000750.

60 V. Fourmond, C. Baffert, K. Sybirna, S. Dementin, A. Abou-Hamdan, I. Meynial-Salles, P. Soucaille, H. Bottin and C. Léger, The Mechanism of Inhibition by H₂ of H₂-Evolution by Hydrogenases, *Chem. Commun.*, 2013, **49**(61), 6840–6842, DOI: 10.1039/c3cc43297a.

61 N. Chongdar, J. A. Birrell, K. Pawlak, C. Sommer, E. J. Reijerse, O. Rüdiger, W. Lubitz and H. Ogata, Unique Spectroscopic Properties of the H-Cluster in a Putative Sensory [FeFe] Hydrogenase, *J. Am. Chem. Soc.*, 2018, **140**(3), 1057–1068, DOI: 10.1021/jacs.7b11287.

62 H. Land, P. Ceccaldi, L. S. Mészáros, M. Lorenzi, H. J. Redman, M. Senger, S. T. Stripp and G. Berggren, Discovery of Novel [FeFe]-Hydrogenases for Biocatalytic H₂-Production, *Chem. Sci.*, 2019, **10**(43), 9941–9948, DOI: 10.1039/c9sc03717a.

63 N. Chongdar, K. Pawlak, O. Rüdiger, E. J. Reijerse, P. Rodriguez-Maciá, W. Lubitz, J. A. Birrell and H. Ogata, Spectroscopic and Biochemical Insight into an Electron-Bifurcating [FeFe] Hydrogenase, *J. Biol. Inorg. Chem.*, 2020, **25**, 135–149, DOI: 10.1007/s00775-019-01747-1.

